El Niño-Southern Oscillation Complexity

Axel Timmermann[1,2,3], Soon-Il An[4], Jong-Seong Kug[5], Fei-Fei Jin[6], Wenju Cai[7,8,9], Antonietta Capotondi[10,11], Kim Cobb[12], Matthieu Lengaigne[13], Michael J. McPhaden[14], Malte F., Stuecker[15,16], Karl Stein[1,2], Andrew T. Wittenberg[17], Kyung-Sook Yun[1,2], Tobias Bayr[18], Han-Ching Chen[19], Yoshimitsu Chikamoto[20], Boris Dewitte[21], Dietmar Dommenget[22], Pamela Grothe[23], Eric Guilyardi[24,25], Yoo-Geun Ham[26], Michiya Hayashi[6], Sarah Ineson[27], Daehyun Kang[28], Sunyong Kim[5], WonMoo Kim[29], June-Yi Lee[1,2], Tim Li[3,6], Jing-Jia Luo[30], Shayne McGregor[22], Yann Planton[24], Scott Power[30], Harun Rashid[7], Hong-Li Ren[31], Agus Santoso[32], Ken Takahashi[33], Alexander Todd[34], Guomin Wang[30], Guojian Wang[7], Ruihuang Xie[35], Woo-Hyun Yang[5], Sang-Wook Yeh[36], Jinho Yoon[37], Elke Zeller[1,2], Xuebin Zhang[38]

[1] Center for Climate Physics, Institute for Basic Science (IBS), Busan 46241, South Korea

[2]Pusan National University, Busan 46241, South Korea

[3]International Pacific Research Center, University of Hawaii at Manoa, Honolulu, Hawaii, USA.

[4]Department of Atmospheric Sciences, Yonsei University, Seoul, Korea

[5]Division of Environmental Science & Engineering, Pohang University of Science and Technology (POSTECH), Pohang 37673, South Korea

[6]Department of Atmospheric Science, SOEST, University of Hawaii at Manoa, Honolulu, Hawaii, USA

[7]CSIRO Oceans and Atmosphere, Aspendale, Victoria 3195, Australia

[8]Physical Oceanography Laboratory/CIMST, Ocean University of China and Qingdao National Laboratory for Marine Science and Technology, Qingdao 266003, China

[9]Centre for Southern Hemisphere Oceans Research (CSHOR), CSIRO Oceans and Atmosphere, Hobart 7004, Australia

[10]Cooperative Institute for Research in Environmental Science, University of Colorado, Boulder CO, 80309, USA

[11]Physical Sciences Division, NOAA Earth System Research Laboratory, Boulder CO, 80305, USA

[12]Earth & Atmospheric Sciences, Georgia Tech, MC 0340 311 Ferst Drive Atlanta, USA

[13]Sorbonne Universités (UPMC, Univ. Paris 06) CNRS-IRD-MNHN, LOCEAN laboratory, IPSL, Paris, France

[14]Pacific Marine Environmental Laboratory/NOAA, Seattle Washington, USA

[15]Department of Atmospheric Sciences, University of Washington, Seattle, Washington, USA

[16]Cooperative Programs for the Advancement of Earth System Science, University Corporation for Atmospheric Research, Boulder, Colorado, USA

[17]Geophysical Fluid Dynamics Laboratory/NOAA, Princeton, New Jersey 08540-6649, USA.

[18]GEOMAR Helmholtz Centre for Ocean Research Düsternbrooker Weg 20, 24105 Kiel, Germany

[19]Department of Atmospheric Sciences, National Taiwan University, Taipei, Taiwan

[20]Department of Plants, Soils, and Climate, Utah State University, Utah, USA

[21]Centro de Estudios Avanzado en Zonas Áridas (CEAZA), Coquimbo, Chile. & Laboratoire d'Etudes en Géophysique et Océanographie Spatiale, Toulouse, France

[22]School of Earth, Atmosphere and Environment, Monash University, Clayton, Australia

[23]Department of Earth and Environmental Sciences, University of Mary Washington, Fredericksburg, VA, USA

[24]Laboratoire d'Océanographie et du Climat: Expérimentation et Approches Numériques (LOCEAN), IRD/UPMC/CNRS/MNHN, Paris Cedex 05, France.

[25]NCAS-Climate, University of Reading, Reading RG6 6BB, UK
[26]Department of Oceanography, Chonnam National University, Gwangju, South Korea
[27]Met Office Hadley Centre, FitzRoy Road, Exeter, EX1 3PB, U.K.
[28]School of Urban and Environmental Engineering, Ulsan National Institute of Science and Technology, 44919, Ulsan, South Korea.
[29]Climate Prediction Department, APEC Climate Center, Busan, Korea,
[30]Australian Bureau of Meteorology, Melbourne, Australia
[31]Laboratory for Climate Studies, National Climate Center, China Meteorological Administration, Beijing, China
[32]ARC Centre of Excellence for Climate System Science, Faculty of Science, University of New South Wales, Sydney, NSW 2052, AUSTRALIA
[33]Instituto Geofisico del Peru, Lima, Peru
[34]University of Exeter College of Engineering, Mathematics and Physical Sciences, Exeter, UK
[35]Institute of Oceanology, Chinese Academy of Sciences, Qingdao, P. R. China
[36]Department of Marine Sciences and Convergent Technology, Hanyang University, Ansan, South Korea
[37]School of Earth Sciences and Environmental Engineering, Gwangju Institute of Science and Technology, Gwangju, 61005, South Korea
[38]CSIRO Ocean and Atmosphere, Hobart TAS 7001, Australia
*Correspondence to: Axel Timmermann. IBS Center for Climate Physics, Pusan National University, Busan, South Korea (E-mail: timmermann@pusan.ac.kr).

El Niño events are characterized by tropical Pacific surface warming and weakening of trade winds occurring every few years. Such conditions are accompanied by changes in atmospheric and oceanic circulation, affecting global climate, marine and terrestrial ecosystems, fisheries and human activities. The alternation of warm El Niño and cold La Niña conditions, referred to as the El Niño-Southern Oscillation (ENSO), represents the strongest year-to-year fluctuation of the global climate system. Here we provide a synthesis of our current understanding of the spatio-temporal complexity of this important climate mode and its influence on the earth system.

1) Introduction

Originally described in 1893 as "*corriente del Niño*"[1] – a warm regional ocean current that affected climate off the coast of Peru – the view on the El Niño phenomenon has changed over the past century. In the 1960s ENSO was recognized as a basin-scale phenomenon involving coupled atmosphere-ocean processes[2]. A major international research program in the 1980s and 90s fundamentally advanced the ability to observe, understand and predict ENSO and its world-wide impacts[3]. During the past 20 years the understanding has continued to evolve as new layers of complexity (Box 1) were identified in ENSO dynamics and predictability. The concept of El Niño has developed from one of a canonical progression of phases from onset, maturity and demise[4] (Fig. 1) to one that accounts for its spatio-temporal complexity (Fig. 2) and varying climatic impacts[5-8] (Fig. 3). We have also come to realize that although

ENSO primarily manifests itself as a year-to-year climate fluctuation, its dynamics involves a broad range of processes interacting on timescales from weeks[9,10] to decades[11]. Here the diversity in patterns, amplitude and temporal evolution of this climate phenomenon will be referred to as "ENSO Complexity" (Box 1).

The most recent El Niño[12] in 2015/16 was initiated in boreal spring by a series of Westerly Wind Events (WWE) (Box 1, Fig. 3e) – a form of tropical weather noise. The associated wind forcing triggered downwelling oceanic Kelvin waves (Box 1, Fig. 1), reducing the upwelling of cold subsurface waters in the Eastern Pacific Cold Tongue (Box 1) and leading to a central and eastern Pacific surface warming. The positive Sea Surface Temperature Anomaly (SSTA) shifted atmospheric convection from the Western Pacific Warm Pool (Box 1) to the central equatorial Pacific, causing a reduction in equatorial trade winds, which in turn intensified surface warming through the positive Bjerknes feedback (Box 1). The seasonally-paced termination of the 2015/16 event (Fig. 3e) was associated with ocean dynamics and the slow discharge of equatorial heat into off-equatorial regions, thus providing a delayed negative feedback (Box 1). The event started to decline in early 2016 and transitioned into a weak La Niña in mid 2016.

In broad terms this evolution is common to the other strong El Niño events in 1982/83 and 1997/98 (Fig. 3c). However, no two events are alike – be they strong, moderate or weak (Fig. 2, 3 f-m). This diversity arises from the varying roles of noise forcing (Fig. 3c-e) and of positive and negative coupled atmosphere/ocean feedback processes[13] (Box 1) that act to enhance and suppress growth of SST anomalies, respectively. The complexity of ENSO (Box 1), along with internal atmospheric noise also translates into a diversity of global impacts[7,14]. When the underlying SSTs change in the equatorial Pacific, there are shifts in atmospheric deep convection, which in turn cause adjustments of the global Walker Circulation (Box 1) and generate stationary atmospheric waves[15] that impact the far reaches of our planet. This perturbed global circulation influences weather variability leading to massive reorganizations of tropical and extratropical temperature and rainfall patterns[16,17] (Fig. 3f-m).

Paleo-climate reconstructions of the ENSO phenomenon covering the past ~10,000 years also show a wide range of amplitudes[18], thus highlighting the importance of internal climate processes in modulating ENSO's complexity on timescales ranging from decades to centuries. In addition, the activity of reconstructed ENSO variability shows an intensification in the late 20th Century relative to other pre-industrial periods[18,19], thus raising the general question of whether external forcings could influence ENSO's evolution and amplitude. How ENSO responds to greenhouse warming is one of the most

compelling outstanding questions[20].

Given the societal and environmental relevance of ENSO, it is paramount to improve our understanding of the processes that control ENSO's amplitude, timing, duration, predictability and global impacts. Here we synthesize our current understanding of ENSO dynamical processes and their role in controlling complexity of this fundamental climate feature. Against this backdrop we will highlight areas of uncertainty (section 6) as a stimulus for further research.

2) A conceptual view of ENSO dynamics

Early efforts to elucidate the dynamics of ENSO focused on the average (composite) evolution of El Niño events[21], capturing the typical evolution of ocean and atmosphere conditions from early spring initiation of El Niño to a wintertime peak and transition to La Niña during the subsequent summer (Fig. 1). The enhanced spectral interannual variability of ENSO (Fig. 3a,b) has been explained by invoking positive atmosphere/ocean feedbacks and delayed negative ocean adjustment feedbacks (Box 1), which together can lead to oscillatory dynamics, as encapsulated by a variety of conceptual ENSO models[22]. Here we focus on the
ENSO recharge oscillator model[23] which in its most general form can be expressed as:

$$dT_e/dt = I_{BJ}\, T_e + F\, h$$

$$dh/dt = -\varepsilon\, h - \alpha\, T_e$$

[equation (1)] where T_e and h represent the equatorial eastern Pacific surface temperature and zonal mean thermocline depth, respectively and dT_e/dt and dh/dt the corresponding time derivatives. The Bjerknes stability index I_{BJ} (referred to as the BJ index or ENSO linear growth rate; Fig. 1j) depends on a number of processes such as thermocline-, zonal advective- and Ekman-feedbacks to reinforce SST, and thermal advection by horizontal mean surface currents and thermal damping by net surface heat fluxes as negative feedbacks[13] (Box 1). In equation (1) ε represents a damping rate of thermocline depth anomalies. The interannual timescale of the ENSO system is mainly determined by F and α, which capture the thermocline feedback (Box 1) and the slow equatorial recharge/discharge process (Box 1) associated with the oceanic heat transport, respectively. For constant I_{BJ} the model describes a linear recharge oscillator: Starting from neutral conditions $T_e \sim 0$ (typically in boreal winter-spring, Fig. 1c, 2) and a charged thermocline state $h>0$, an El Niño can grow (Fig. 1d,e, 2). While eastern equatorial Pacific SSTA develop, the thermocline feedback (Box 1) Fh further intensifies the growth of

SSTA by upwelling anomalously warm subsurface waters to the surface in the Eastern Pacific Cold Tongue. Moreover, positive eastern Pacific SSTA ($T_e>0$) cause a weakening of the equatorial trade winds (Fig. 1d,e). The associated wind-stress curl discharges the equatorial heat through Sverdrup transport (Box 1) and ocean boundary processes (Fig. 1f). The resulting drainage of heat in turn weakens the thermocline feedback, and the phase of the ENSO recharge oscillator can transition into a La Niña state (Fig. 1g,h), which is accompanied by recharging of heat through opposite wind-stress curl anomalies (Fig. 1h).

Comparing the linear oscillator solution of equation (1) ($I_{BJ}=const$) with the scatterplot of observed equatorial eastern Pacific temperature and zonal mean thermocline depth anomalies (Fig. 2), we find substantial differences. The observed scatter diagram shows a high degree of irregularity and a notable positive skewness in eastern tropical Pacific SSTA towards El Niño events (Box 1, Fig. 2). El Niño and La Niña events are very different in terms of their amplitude and time-evolution (Fig. 1k, 2a). To account for this additional level of complexity the simple recharge oscillator model can be extended by including a nonlinear Bjerknes feedback term that represents either atmospheric or oceanic nonlinear processes[24] or multiplicative stochastic forcing[25] (Box 1). For these extensions, the recharge model can then simulate ENSO's skewed probability distribution (Fig. 2) and the fast growth from neutral to strong El Niño conditions (Fig. 1j). The observed positive skewness of SSTA (Fig. 2), which indicates the importance of nonlinear dynamical and thermodynamical processes in the coupled tropical Pacific climate system, implies that strong El Niño conditions, which typically last for 1 year, are on average shorter than La Niña events, which can persist for up to several years (Fig. 1k).

Whereas conceptual models like equation (1) can simulate some key features of ENSO's evolution, they can neither explain the presence of ENSO's spatial diversity (Fig. 3a,b,f-m), nor the potential remote effects of variability originating from the extra-tropical Pacific, Atlantic or Indian Ocean onto this diversity. An improved framework to characterize and explain ENSO complexity is needed to capture these aspects.

3) Space-time complexity of ENSO

In spite of some prominent commonalities discussed in section 2 (Fig. 1), El Niño events differ considerably from each other in terms of magnitude, spatial pattern, temporal evolution, and predictability[5-7] (Fig. 2, 3 f-m). To characterize the leading modes of equatorial Pacific SST variability, and their diverse timescales, we conduct an Empirical Orthogonal Function (EOF) analysis of observed tropical Pacific SSTA[26] (Fig. 3), which identifies the leading orthogonal patterns of variability. The

leading EOF (Fig. 3a), which corresponds to the classical El Niño pattern with eastern tropical Pacific warming, exhibits variability on quasi-quadrennial time scales (3-7 years) (spectral density estimate in Fig. 3a). In contrast, the second EOF, which explains only 25% of the variance of the first mode, is characterized by an east/west zonal SST dipole in the tropical Pacific and has enhanced variance on quasi-biennial and decadal timescales (spectral density estimate Fig. 3b). The interplay of these two EOFs largely captures the spatial diversity of the observed ENSO mode.

Some El Niño events (e.g. 1997/98) (Fig. 3c,f) are characterized by pronounced warming in the Eastern Pacific (referred to as EP El Niño events), while others show a stronger positive projection on the second EOF mode, which leads to a more pronounced Central Pacific warming (referred to as CP El Niño events) (e.g. 2004/05) (Fig. 3d,h,i,j). More generally, El Niño events can be viewed as the superposition of the two EOF modes, resulting in a continuum of ENSO characteristics[27,28] that capture a mix of EP and CP dynamics (e.g. 1991/92 and 2015/16 events) (Fig. 2). La Niña events (e.g. 1999/2000) (Fig. 3g), in addition to being weaker, exhibit less diversity in their spatial patterns[6,29], thus clearly pointing to an asymmetry in the underlying dynamical processes for ENSO.

EP El Niño events (e.g. 1997/98) (Fig. 3c) tend to involve basin-scale equatorial wind anomalies, a strong relaxation of the zonal tilt of the equatorial thermocline (Fig. 1e), a more prominent role for the thermocline feedback (Box 1), large eastward shifts of tropical Pacific convection, and strong discharge of heat content (Fig. 3c) away from the equatorial region, which boosts the likelihood of transitioning into a La Niña event[6,30]. In contrast, CP El Niño events (e.g. 2004/05) (Fig. 3d) tend to involve more local wind feedbacks, a stronger role for the zonal advective feedback (Box 1), little reduction in the zonal tilt of the thermocline, weak shifts of convection, earlier termination, little poleward discharge of ocean heat content (Fig. 3d), a stronger role for thermal damping (Box 1) during the decay phase, a reduced likelihood to transition into La Niña, and more susceptibility to disruption by wind noise[6,30]. Compared to CP El Niños, strong EP El Niños also tend to terminate later in boreal spring, due to a trade wind collapse which suppresses the upwelling that normally connects the SST to the evolving thermocline depth[31].

The spatial diversity in ENSO's SSTA patterns is also associated with different tropical precipitation patterns (Fig. 3f-m), resulting in potentially different remote teleconnection patterns and corresponding weather and climate impacts[7,32]. However, given the high level of internal atmospheric variability[33] and the brevity of the historical record, it has remained difficult to unequivocally detect the differences in the impacts of various ENSO spatial modes. In addition to its spatial diversity, ENSO also

exhibits substantial diversity in its temporal evolution (Fig. 1k, 3 c,d,e). Understanding this diversity of El Niño events is crucial for predicting ENSO's regional impacts, e.g. on precipitation patterns, tropical cyclones, and other severe weather[5]. The extent to which El Niño diversity is predictable relates to whether ENSO's complexity originates mainly from random processes, or from low-frequency deterministic dynamics. Random processes affecting a single physical ENSO mode could generate diversity in amplitude, spatial structure, and temporal evolution[8], consistent with a spatial flavor continuum generated by different realizations of atmospheric noise[27]. Alternatively, initial subsurface ocean conditions could modulate the role of stochastic wind forcing in producing diversity. For example, climate model simulations have demonstrated that in the presence of stochastic WWEs, an initial buildup of equatorial Pacific upper-ocean heat content can favor the development of EP rather than CP El Niño events[10,34] (Fig. 3d,e). At the onset of strong El Niño events[35] such as 1997/98 and 2015/16 (Fig. 3c,e), WWE activity tends to strengthen and expand eastward with the expansion of the Western Pacific Warm Pool and the relaxation of the trade winds. These WWE changes can be parameterized in equation (1) as multiplicative noise (Box 1), which can contribute to ENSO diversity and asymmetries[9,36].

Studies suggest that ENSO diversity may be triggered by climate phenomena outside the tropical Pacific, including the North[37] and South Pacific[38] meridional modes, extra-tropical atmospheric circulation patterns, and tropical Atlantic variability[5,39,40]. For example, the negative phase of the North Pacific Oscillation[41] tends to favor the development of positive SST anomalies in the central Pacific by weakening the trade winds in the northern Hemisphere, while the positive phase of the South Pacific Oscillation tends to weaken the southern Hemisphere trades, thereby favouring the development of positive SSTAs in the eastern Pacific. Such remote influences appear to be mediated primarily by how they project onto wind variations in the equatorial Pacific. In essence, westerly wind anomalies in the western equatorial Pacific tend to favor CP El Niños, while westerly wind anomalies in the central-eastern equatorial Pacific tend to favor EP El Niños. These external influences can precede the peak of El Niño by 2-3 seasons[39,41] and may provide additional predictability to the spatial characteristics of an emerging El Niño event.

Since 1998, CP events have been more prevalent than EP events[42]. Such a decadal modulation in ENSO diversity is consistent with CGCMs that can spontaneously generate multidecadal variations in ENSO diversity even in the absence of external radiative forcings[43]. Low-frequency climatic drivers (including natural and anthropogenic forcings) — which involve basinwide changes in the zonal SST gradient, thermocline depth, and winds[44,45] — may also have contributed to the observed decadal swings in

ENSO diversity by favoring particular spatio-temporal modes[46]. At this stage, the observational record remains too short to quantify all the possible sources of the decadal modulation of ENSO characteristics.

The current generation of climate models underestimates ENSO diversity[47]. This issue is related to the models' systematic biases, which affect the mean state and ENSO feedbacks. Sources of these biases include deficiencies in the simulation of clouds, atmospheric convection, and oceanic mixing[48]. In particular, atmospheric model responses tend to be relatively insensitive to distinct patterns of SST anomalies, due to climatological dry and cold biases in the equatorial central Pacific[47,49].

4) Seasonal ENSO dynamics

ENSO displays a close relationship with the seasonal cycle[21,50]: El Niño events usually start in boreal spring (Fig. 1c,i, 4), grow during the summer and fall (Fig. 1d), reach their maximum intensity in winter (Fig. 1e,i), and decay rapidly during late winter and spring (Fig. 1f,j). In most cases, by the subsequent summer, they transition to La Niña events (Fig. 1g,h, 4). This seasonal synchronization of ENSO translates into the observed eastern equatorial Pacific SSTA variance peaking during boreal winter and attaining minimum values during spring (Fig. 1j). It also leads to pronounced seasonal contrasts in ENSO's climate impacts and predictability (Fig. 1i). ENSO influences the global atmospheric circulation, affecting for instance the Asian Monsoons[51], climate in America[52], and Australia[53].

Randomly occurring sequences of WWEs, typically during spring, can lead to an initial warming of the central-eastern equatorial Pacific[54,55] (Fig. 1c). This initial SSTA can grow because the air-sea coupling is strongest in summer and early fall[56,57] (Fig. 1j). Proposed physical processes for this summer/fall coupling maximum include (i) the equatorward shift of the ITCZ and its associated increase in western Pacific surface wind convergence[58], (ii) the seasonal outcropping of the equatorial thermocline[59], (iii) the seasonal cooling of the eastern equatorial Pacific[58], (iv) and the reduction of the negative cloud feedbacks[60].

The decay of El Niño events typically starts in boreal winter. The anomalous westerlies shift southward from the equator, leading to a shoaling of the eastern Pacific thermocline, and a subsequent reduction of the overlying SSTA[61] (Fig. 1f, 4a). This shift arises from climatological expansion of the Western Pacific Warm Pool into the Southern Hemisphere, coincident with the development of the South Pacific Convergence Zone[62]. In this season, the increased surface heat flux damping[60] results in a decrease of the air-sea coupling strength (Fig. 1j), which together with the aforementioned seasonal southward

283 wind shift[63] and the equatorial heat content discharge[23] (Fig. 4b) lead to a rapid transition to a La Niña
284 state.
285
286 While these seasonal processes generally operate for different flavors and phases of ENSO, differences
287 in their relative importance can contribute to ENSO complexity. For instance, CP events typically
288 terminate earlier and are less likely to transition to a La Niña state compared to EP El Niño events[62]
289 (Fig. 3d). Furthermore, La Niña conditions can last up to 2-3 years (Fig. 3c, 4b). The ability to simulate
290 ENSO seasonal synchronization for different types of El Niño events varies strongly among the current
291 generation of climate models, likely due to biases in mean state and seasonal cycle[56].
292
293 The influence of the seasonal variations of the air-sea coupling strength discussed above can be included
294 in the framework of the recharge oscillator [equation (1)] by adding a seasonally varying growth rate
295 (I_{BJ}). As expected, this model then captures the observed ENSO seasonal synchronization
296 characteristics, including the seasonal ENSO variance modulation and partial phase synchronization[25].
297 Interactions between the seasonal cycle in I_{BJ} and the interannual ENSO temperature signal generate
298 variance with periods at roughly 9 and 15-18 months, the so-called combination tone frequencies (Box
299 1) that broaden the ENSO spectrum predominantly towards higher frequencies[64,65]. These interacting
300 dynamics create specific atmospheric circulation patterns that are together referred to as Combination
301 Mode[64] (C-mode) (Box 1). The spatial pattern of the C-mode exhibits a pronounced hemispheric
302 asymmetry, which includes an anomalous cyclonic low-level wind circulation in the Southern
303 Hemisphere Central Pacific and an anomalous anticyclonic low-level wind circulation in the Northern
304 Hemisphere Western Pacific. Some of prominent local expressions are the aforementioned southward
305 shift of equatorial wind anomalies[63] (Fig. 1e) and the anomalous Western North Pacific Anticyclone[65].
306
307 **5) ENSO predictability**
308 To link our dynamical understanding of tropical air-sea interactions with ENSO predictability, it is
309 helpful to elucidate the seasonal evolution of i) potential precursors that may contribute to long-term
310 predictability[66] (9-15 months lead time), ii) triggers that can rapidly increase the likelihood for event
311 development (6-9 months lead time) and iii) transition processes (section 2, 4). The development of a
312 typical EP event can be divided into different seasonal stages which each contribute differently to the
313 boreal winter Niño 3.4 SSTA forecasting skill of up to 9-6 months, as illustrated by the anomaly
314 correlation coefficient skill between seasonal forecasts performed with the North American Multimodel
315 Ensemble[67] (NMME) and the observations (Fig. 4a, cyan dashed line). Prior to boreal spring a charged
316 western tropical Pacific heat content is a necessary condition for the subsequent development of El Niño

317 events (Fig. 4b). Corresponding warm pool heat advection processes[68,69] thus play a key role in
318 determining the long-term memory for ENSO forecasts. Furthermore, atmospheric precursors in the
319 North[37] and South Pacific[38], the Indian Ocean[70], or the tropical Atlantic[40,71] have been suggested to
320 influence the El Niño evolution for long lead times.
321
322 It must be emphasized here that the presence of such early oceanic or atmospheric precursors is usually
323 not sufficient for El Niño growth, as one of the key trigger mechanisms is the stochastic WWE activity
324 in boreal spring and early summer[72]. This is clearly illustrated by the fact that even though heat content
325 initial conditions were favourable for El Niño development in early 2012, 2014 and 2017, the
326 subsequent SSTA growth stayed below expectations. Individual WWEs are not predictable beyond the
327 weather prediction horizon, which implies that on average forecasts initialized in boreal spring have
328 relatively low long-term skill[73], in particular in the absence of pre-cursor signals (Fig. 4a, cyan line).
329 However, pre-cursor signals in western tropical Pacific heat content (Fig. 4b) could be indicative of
330 potentially developing El Niño conditions, which in effect enhance the predictability (Fig. 4a, orange
331 line) relative to the averaged case (Fig. 4a, cyan line). The competing roles of stochasticity versus ocean
332 memory for this so-called spring predictability barrier (Fig. 4a) and for long-lead time forecasts have
333 been intensely debated[74,75].
334
335 If a sufficient amount of westerly momentum is transferred in boreal spring from the atmosphere to the
336 ocean, zonal advective processes begin moving the warm pool front eastward and downwelling Kelvin
337 waves (Box 1) generate surface warming in the eastern tropical Pacific about 2 months later. These
338 anomalies will be further intensified (Fig. 4a) owing to increasing summer air-sea coupling strength
339 (Fig. 1j), while anomalously warm water is drained from the Western Pacific Warm Pool (Fig. 4b).
340 This phase exhibits a high degree of climate predictability, as documented by the high anomaly
341 correlation coefficients (>0.6) between predicted boreal winter El Niño events and observations for
342 forecasts initialized in boreal summer (Fig. 4a). The subsequent demise of an El Niño event is largely
343 controlled by ocean-subsurface processes and the discharge of zonal heat content away from the equator
344 (Fig. 1i, 2, equation (1)), as well as by the seasonally modulated southward shift of westerly wind
345 anomalies[63], which in turn leads to a relaxation of the zonally integrated thermocline anomalies. This
346 seasonally locked decay of El Niño conditions under a low noise atmospheric environment further
347 contributes to the long-term averaged ENSO prediction skill[62].
348
349 The subsequent evolution into a La Niña state (Fig. 4a, b, c) and the possibility to have multi-year La
350 Niña events (Fig. 1k, 4c) are less well understood. La Niña events are often preceded by a strong El

Niño. However, as indicated by the broad probability distribution of SSTA at lag 9-15 months (Fig. 4c), other initial conditions can also develop into La Niña events peaking in boreal winter (Fig. 4c). During the transition from El Niño to La Niña equatorial heat gets quickly discharged and 6-9 months prior to a peak La Niña in boreal winter, we observe the smallest values of the equatorial heat content (Fig. 1i) and a slow recharging tendency of the Western Pacific Warm Pool (Fig. 4d). However, also during this period the probability density of western tropical Pacific heat content anomalies is relatively broad, which translates into an overall reduction of predictive skill (Fig. 4c). As longer-lasting La Niña events are exposed to a variety of atmospheric and oceanic perturbations and the annual cycle, a dynamical decoupling of La Niña and subsequent El Niño events may occur[76]. In boreal winter, during the peak of the La Niña, the Western Pacific Warm Pool is fully charged (Fig. 4d) to values that are typical for an El Niño pre-cursor (Fig. 4b). However, the SST conditions do not necessarily have to swing back to an El Niño state and sometimes even a second subsequent La Niña can develop. Comparing the anomaly correlation coefficient skill for December La Niña target conditions with the averaged skill for all years (1980-2015) from the NMME[77], we find very little difference (Fig. 4c) for lead times 1-12 month, which suggests i) that La Niña conditions have a considerably lower predictability than El Niño, ii) the predictability of La Niña is to a first order captured well by the mean statistical skill of the current generation of seasonal prediction models. Using ensemble forecasting techniques, a recent study[78] identified potential predictors for the likelihood of multi-year La Niña events, which include the magnitude of thermocline discharge and the amplitude of the preceding El Niño event, suggesting the possibility for longer-term forecasts also for La Niña.

How the different stages of predictability differ between CP and EP events and whether there are distinct precursor patterns for different ENSO flavors still remains controversial[68,79]. Despite an improved understanding of ENSO dynamics, ENSO prediction skill has not demonstrated a steady improvement during the past few decades, with even a decrease of ENSO prediction skill at the turn of the 21st Century[73]. This decrease may be related to the reduced ENSO amplitude and the more frequent occurrence of CP events during that period[79], as their evolution and climate impacts tend to be less predictable than those of EP El Niño events[80].

6) A unifying framework

The discussions in previous sections have highlighted a variety of dynamical pathways that can be synthesized to explain the spatio-temporal complexity of the ENSO phenomenon (Fig. 5). Extending beyond the simple single mode theory (equation (1), section 2), which captures several features of ENSO dynamics, but not all, our proposed framework for ENSO complexity is based on the co-

existence of a duplet of linear eigenmodes (Fig. 5 a,b), which can be derived from a deterministic intermediate complexity tropical atmosphere/ocean model[46], and a number of excitation mechanisms. These two generic coupled eigenmodes are characterized by spatial patterns that closely resemble the observed EP and CP modes (Fig. 5) and by timescales of approximately 4 and 2 years, respectively. The 4-year (quasi-quadrennial, QQ) mode is more prominent (Fig. 5, lower left) when the mean thermocline is deep and the tradewinds are weak. It relies strongly on the thermocline feedback. In contrast, the 2-year mode (quasi-biennial, QB) is dominant when the mean thermocline is shallow and the equatorial trade winds are strong. Its SST variability is strongly controlled by the zonal advective feedback[46]. These features are akin to their observational counterparts (Fig. 3, 5 c,d). For realistic background states both modes operate not far away from criticality (zero growth rate) (Fig. 5, lower left), which implies that they can be easily excited by other processes. Their stability and excitability depends further on the prevailing climatic background conditions.

At the heart of our explanation for ENSO's *spatial* flavors is the aforementioned multiplicity of coupled ENSO eigenmodes (Fig. 5 a,b), as seen in this specific ENSO model[46]. Furthermore, the *temporal* complexity is generated in part by the different oscillation frequencies of the QQ and QB modes and additionally by different external excitation processes associated e.g. with the North and South Pacific Meridional Modes[81,82], the South Pacific booster[38], Westerly Wind Events (section 3,4), Tropical Instability Waves[83], or transbasin influences[40] (Fig. 5). In particular, asymmetric dependencies related to the increased Westerly Wind event activity during El Niño and enhanced Tropical Instability Wave activity during La Niña make these cross scale interactions very effective sources for ENSO complexity. Furthermore, the annual cycle of winds and SST plays a key role in determining the seasonal timing of ENSO anomalies and its predictability (section 4, 5). To further explain the fact that El Niño anomalies are stronger in amplitude (section 2) and exhibit a more pronounced spatial diversity (section 3), and higher predictability[84] relative to their La Niña counterparts (Fig. 4,b,d, 5c,e), we need to invoke additional nonlinear processes. Nonlinearities, particularly in atmospheric deep convection and oceanic heat advection, can induce a wide range of additional timescales[64] and new spatial structures[85,86] by potentially coupling and/or amplifying the duplet of ENSO eigenmodes.

Decadal subsurface processes[87,88] can affect the long-term climatological background state. In turn this will change the stability of the two primary ENSO eigenmodes (Fig. 5 a,b) and their excitability. Hence, slow background state changes in the Pacific Ocean can play a key role in generating and modulating ENSO's spatio-temporal complexity.

Our synthesis framework for ENSO complexity (Fig. 5), which identifies key ingredients for ENSO complexity (primary ENSO eigenmodes, excitation processes, nonlinearities and cross-timescale interactions), may serve as a roadmap for further hypotheses testing, process studies and diagnostic analysis of climate models. It can help guide the evolution of the tropical Pacific observing system, which is essential for underpinning ENSO research and forecasting[89]. In addition, this framework can be used to determine how the shortcomings in representing ENSO complexity in climate and earth system models are related to a variety of feedback processes and biases in the mean state and annual cycle that affect the generation of climate variability.

7) Outlook

The reliability of dynamical seasonal climate predictions depends heavily on the representation of ENSO processes in CGCMs and also on the continuous improvement of the global ocean observing system. Climate models still exhibit stubborn climate biases in the eastern equatorial Pacific[90] that may impact their representation of feedbacks (section 2), ENSO complexity[47], and in turn may affect the fidelity of operational ENSO forecasts. Identifying and resolving underlying systematic model biases will help in developing the next generation of models for seamless climate forecasts and projections.

Future research on ENSO complexity needs to address the role of the seasonal cycle for CP ENSO dynamics, the near-absence of spatial diversity for La Niña[29] (Fig. 5e), the impact of decadal background state changes on ENSO modes vis-à-vis multiple-timescale processes involving Westerly Wind Events, Tropical Instability waves, extratropical triggers as well as the response of ENSO's spatio-temporal complexity to past and future climate change. Moreover, it needs to be studied, whether the underlying dynamical origin for spatial-temporal diversity in CGCMs can in fact be linked to the duplet of QQ and QB ENSO eigenmodes, described in section 6. This can be tested by applying interactive atmosphere ensemble averaging techniques in coupled climate models[91], which artificially reduce non-SST-related atmospheric perturbations. Moreover, the use of flux-adjusted CGCMs[92] could help elucidate how model biases impact ENSO's spatial diversity and provide a more effective way of improving seasonal climate predictions. Such experiments could further reveal if there are distinct precursors for ENSO diversity, which could be used to further inform ENSO forecasts. Much scientific emphasis has been placed on understanding the growth of El Niño events. However, given the severe impacts of La Niña e.g. on drought in the Southwestern United States[93] or the Horn of Africa[94], and the fact that La Niña events may last longer than one year (Fig. 4), it will be paramount to gain also deeper understanding of the processes controlling La Niña and its predictability through observational, diagnostic and modeling studies.

A growing global population in the 21st century has become increasingly vulnerable to natural hazards as human activities alter the climate and the environment. Society therefore has an urgent demand for better climate products and services, including improved ENSO monitoring and predictions and long term projections, to better inform decision-making for agriculture and food security, public health, water resource management, energy production, human migration, and disaster risk reduction. ENSO is a unifying concept in earth system science[95]. Thus, our proposed synthesis for ENSO complexity (sections 2-5) can serve as both a catalyst to further research and, in its practical applications, an essential contributor for sustainable development and environmental stewardship in a changing world.

Fig. 1| ENSO Cycle: Composite evolution of El Niño events from 1958 to 2015. a) Mean sea surface temperature[26] (SST) and b) subsurface potential temperature[96] between 2°N and 2°S. The depth of the 20°C isotherm (Z20) is indicated by the black line. (c-h) Composite SST anomalies[26] (SSTA) and subsurface temperature anomalies[96] from 17 El Niño events (1963, 1965, 1968, 1969, 1972, 1976, 1977, 1982, 1986, 1987, 1991, 1994, 1997, 2002, 2004, 2006, 2009), based on the 0.5°C exceedance of the three month running mean of NOAA ERSST.v5 SST anomalies[97] in the Niño3.4 region (averaged over 5°S-5°N, 120°W-170°W). The arrows schematically represent wind anomalies and the boxes list major processes involved in the phases of El Niño evolution. (i) The composite means (lines) and spread (shading) of Niño3 SSTA (red, averaged over 5°S-5°N, 90°W-150°W,) and equatorial Pacific zonal mean Z20 (blue) for the 17 El Niño events. The diamond illustrates that ENSO predictability increases with increasing ENSO signal strength. (j) The monthly standard deviation (SD) of Niño3 SSTA[26] (red line) and an estimate of monthly ENSO growth rate based on the Bjerknes stability index[56]. (k) Time series of Niño3 SSTA and zonal mean equatorial Pacific depth anomaly from 20°C isotherm (from 2°S-2°N, 120°E-80°W) from merged data product[27,98].

Fig. 2: | Schematic representation of ENSO temporal complexity. Kernel density estimate of the joint probability distribution (orange shading) of linearly detrended Niño3 SSTA and zonal mean 20°C isotherm depth anomalies (from 2°S-2°N, 120°E-80°W) for the period 1958-2016 from a merged data product[27,98]. The gray circles indicate the monthly values of the two time series, smoothed with a 3-month running mean filter. Dark and light blue triangles indicate December values of EP (1972, 1976, 1982, 1986, 1997, 2006, 2015) and CP El Niños (1968, 1994, 2009), respectively. Mixed events (1965, 1991, 2002) are represented by combined dark and light blue triangles. The years

for the four largest El Niño events are indicated. The white ellipse in the center corresponds to the progression of the linear recharge oscillator, and arrows on the left and right indicate (dis)charging of subsurface warm water in the equatorial Pacific.

Fig. 3. Spatio-temporal complexity of ENSO. 1st (a) 2nd (b) EOF patterns of linearly detrended SSTA[95] computed for 25°S-25°N, 140°E-80°W during 1920-2016, with associated variance-preserving spectral power density on the left (vertical axis is period in years, horizontal axis is log power); c,d,e) longitude-time evolution of Pacific SSTA averaged 5°S-5°N, for selected observed ENSO events, with 28.5°C isotherm of SST (red curve) representing the edge of the Western Pacific Warm Pool, longitude and strength of WWEs[99] (black circles), and (on the left) associated equatorial Pacific heat content anomaly (temperature anomaly averaged over the top 300 m of the ocean and between 5°S-5°N and 120°E-90°W; range from -1 to 1K; red positive, blue negative). (f-m) spatial pattern of SSTA (shaded) and precipitation anomaly[100] (contours, positive solid, negative dashed, 2 mm/day interval, zero contour omitted) averaged over the Nov-Dec-Jan season of selected ENSO events. Note that strong warm events (1997/98, 2015/16) induce very strong eastward and equatorward shifts of rainfall. Bottom-right of each panel of (a,b,f-m): associated principal components (PCs), namely the projection of each SSTA spatial pattern onto the EOF patterns in (a,b); abscissa is PC1, ordinate is PC2, and arrow length is relative to the unit circle.

Fig. 4 | Probabilistic ENSO pre-cursors and predictive skill. Time-evolving Kernel density probability density estimates (shading) of linearly detrended Niño3.4 SSTA[26] for the period 1958-2016 for a.) El Niño and c.) La Niña conditions, exceeding the +/-0.5°C threshold (White/transparent shading), respectively. b.) and d.) same as a.), c.), but for western tropical Pacific heat content anomalies[96] (temperature anomalies averaged from 5°S-5°N, 120°E-155°W and 0-300 m and high-pass filtered with a cut-off period of 20 years to remove multi-decadal trends). For every time the probability for SSTA (heat content anomalies) to be in the range of -3 to 3°C (-2 and 2°C) is ~100%. However, some SSTA and heat content values are more likely to occur than others. This is indicated by the colored shading. The time-evolution of the probability density estimates is shown for different lead and lag times, relative to El Niño and La Niña events peaking in December. Colored thin lines correspond to the maximum probability for each lag. Thick lines in a.) represent the anomaly correlation coefficient skill (ACC) for December Niño3.4 SSTA[97] (1980-2015) exceeding +0.5°C (orange), within the range +/-0.5°C (gray) and for all years (cyan) calculated using 9 coupled models from the North American Multimodel Ensemble project[77]. Lines in c.), same as a.), but for anomalies

519 below -0.5°C (blue), within the range +/-0.5°C (gray) and all years (cyan). Note the ACC shown here
520 in orange and blue lines does not represent the skill aggregated over all initial conditions, but only over
521 those identified a posteriori as El Niño and La Niña events.
522
523 **Fig. 5 | Mechanisms for ENSO Complexity.** Top two left panels: Leading 2 eigenmodes of SSTA
524 (°C) and equatorial thermocline depth anomalies (averaged between 5°S-5°N) with periods of ~4 (QQ)
525 and ~2 (QB) years, calculated fom an intermediate ENSO model[46]. The differences in zonal location of
526 the center in SSTA and thermocline anomalies are largely due to different roles of the zonal advective
527 feedback (ZAF) and thermocline feedback (TF). Bottom left panels: growth rates of two eigenmodes as
528 a function of mean thermocline depth and the strength of mean equatorial trade winds relative to
529 climatological conditions. Black dots mark the mean state for the modes displayed in the upper left
530 panels. Right panels: patterns of SSTA[26] and equatorial TAO/TRITON 20°C thermocline depth
531 anomalies for typical EP (1997/98), CP (2009/2010) El Niño, and La Niña (boreal winter 2010)
532 events (Nov-Dec-Jan) with schematic representation of key excitation, nonlinear and cross-scale
533 interaction mechanisms: annual cycle (ACY), Westerly Wind Events (WWE), South Pacific Booster
534 (SPB), North and South Pacific Meridional Modes (NPMM, SPMM) and Tropical Instabilty Waves
535 (TIW). The solid red-eastward (blue-westward) arrows represent the ZAF and red-upward (blue-
536 downward) TF for El Niño (La Niña) conditions, respectively. The relative sizes and different zonal
537 positions of the arrows indicate qualitatively the strength and areas of strong feedback efficiency. Curly
538 upward (downward) arrows denote damping net surface heat flux feedback for El Niño (La Niña).
539
540
541 **Box 1| ENSO Glossary:**
542
543 **Bjerknes feedback:** Positive ENSO feedback along the equator, in which a weakened (strengthened)
544 equatorial zonal SST gradient weakens (strengthens) trade winds, which in turn further reduces
545 (increases) the zonal SST gradient.
546 **Combination Tones / C-mode:** Enhanced spectral energy on timescales of 9 months and 15-18
547 months, generated by the nonlinear modulation of ENSO by the seasonal cycle, and vice versa. C-
548 modes play an important role in the seasonal turnabout of El Niño events.
549 **Eastern Pacific Cold Tongue:** An eastern equatorial Pacific region characterized by wind-driven
550 upwelling of cold subsurface waters (Fig. 1a,b). The Cold Tongue warms considerably during Eastern
551 Pacific (EP) El Niño events, and cools during La Niña events.

552 **Ekman Feedback:** Positive (negative) SST anomalies weaken (strengthen) the equatorial trade winds,
553 reducing (increasing) the upwelling of cold subsurface water in the eastern equatorial Pacific, thus
554 reinforcing the original SST anomaly.
555 **ENSO Complexity**: Complexity expands on the concept of ENSO "pattern diversity" to include also
556 temporal characteristics (from weather, annual cycle, interannual to decadal timescales), dynamics,
557 predictability and global impacts
558 **ENSO Skewness:** Amplitude asymmetry of El Niño and La Niña events, which quantifies the fact that
559 El Niño events attain larger amplitudes than La Niña events. Skewness is clear a indication of
560 nonlinearity in the ENSO cycle.
561 **Equatorial Kelvin Wave:** Eastward propagating oceanic internal wave that displaces the interface
562 (thermocline) between warm surface waters and cold subsurface waters. Westerly (easterly) equatorial
563 wind anomalies generate downwelling (upwelling) Kelvin waves, which deepen (shoal) the thermocline
564 in the eastern Pacific and reduce (enhance) the efficiency of climatological upwelling.
565 **Multiplicative Noise:** Interaction between Westerly Wind Events (WWEs) and underlying SST in
566 the western and central Pacific, in which warmer (colder) SST favors more (fewer) WWEs, also
567 referred to as state-dependent noise.
568 **Recharge/Discharge**: Meridional transport of heat into/out of equatorial band driven by changes in
569 near-equatorial wind variations. Recharge/discharge processes play key role in initiation and
570 termination of El Niño events.
571 **Thermal damping**: Typically a negative feedback arising from SST-induced changes in surface
572 radiative and turbulent heat fluxes in the tropical Pacific. It involves tropical clouds, convection and
573 atmospheric boundary layer physics.
574 **Thermocline feedback**: Generally positive feedback operating in the eastern equatorial Pacific, in
575 which a warm (cold) equatorial SSTA weakens (strengthens) equatorial trade winds, leading to mean
576 upwelling of anomalously warm (cold) water.
577 **Westerly Wind Event:** Weather systems in the western and central Pacific, that are often associated
578 with an abrupt relaxation of the equatorial trade winds, generating downwelling Kelvin waves and an
579 eastward expansion of the Western Pacific Warm Pool.
580 **Western Pacific Warm Pool:** Some of the warmest waters in the worlds' oceans occur in the
581 western tropical Pacific with temperatures exceeding 28°C (Fig. 1a,b). The Warm Pool's seasonal
582 north-south migrations play an important role in the termination of El Niño events.

583 **Zonal-advective feedback**: Positive feedback, particularly effective in the central Pacific, in which a
584 positive (negative) equatorial SSTA weakens (strengthens) equatorial trade winds, reducing (enhancing)
585 the oceanic transport of cold waters from the eastern Pacific.
586
587
588 **Acknowledgements:**
589 AT, KJS, KSY, EZ were supported by the Institute for Basic Science (project code IBS-R028-D1). BD
590 was funded by Fondecyt (grant 1151185). SIA was supported by Basic Science Research Program
591 through National Research Foundation of Korea (NRF-2017R1A2A2A05069383). JSK was supported
592 by the National Research Foundation of Korea (NRF-2017R1A2B3011511). FFJ's contribution was
593 sponsored through U.S. NSF Grant AGS-1406601 and U.S. Department of Energy Grant DE-
594 SC0005110. TB receives funding from SFB 754 "Climate-Biochemistry Interactions in the tropical
595 Ocean". MJM is supported by NOAA. HLR is supported by China Meteorological Special Research
596 Project (grant number: GYHY201506013). SI was supported by the UK-China Research & Innovation
597 Partnership Fund through the Met Office Climate Science for Service Partnership (CSSP) China as part
598 of the Newton Fund. MFS acknowledges support from NOAA Climate and Global Change Postdoctoral
599 Fellowship Program, administered by UCAR's Cooperative Programs for the Advancement of Earth
600 System Sciences (CPAESS). HR was partly funded by the National Environmental Science Program,
601 Australia. This is PMEL contribution number 4723. The authors thank the TAO Project Office of
602 NOAA/PMEL for providing the TAO/TRITON 20°C isotherm depth anomaly data in Fig.5.
603
604 **Competing interests**: The authors declare no competing interests.
605
606
607 **References**
608
609 1 Carrillo, C. N. Hidrografía oceánica. *Bol Soc Geogr Lima*, 72-110 (1893).
610 2 Bjerknes, J. Atmospheric Teleconnections from the Equatorial Pacific. *Monthly Weather Review*
611 **97**, 163-172 (1969).
612 3 McPhaden, M. J., Busalacchi, A. J. & Anderson, D. L. T. A TOGA Retrospective.
613 *Oceanography* **23**, 86-103, doi:10.5670/oceanog.2010.26 (2010).
614 4 Cai, W. J. *et al.* More extreme swings of the South Pacific convergence zone due to greenhouse
615 warming. *Nature* **488**, 365-369, doi:10.1038/nature11358 (2012).

5 Capotondi, A. *et al.* Understanding ENSO Diversity. *Bulletin of the American Meteorological Society* **96**, 921-938, doi:10.1175/bams-d-13-00117.1 (2015).

6 Kug, J. S., Jin, F. F. & An, S. I. Two Types of El Niño Events: Cold Tongue El Niño and Warm Pool El Niño. *Journal of Climate* **22**, 1499-1515, doi:10.1175/2008jcli2624.1 (2009).

Demonstrates that the two types of El Niño (CP and EP) have different dynamical structures including discharge processes and dominant SST feedbacks.

7 Ashok, K., Behera, S. K., Rao, S. A., Weng, H. Y. & Yamagata, T. El Niño Modoki and its possible teleconnection. *Journal of Geophysical Research-Oceans* **112**, doi:10.1029/2006jc003798 (2007).

8 Takahashi, K., Montecinos, A., Goubanova, K. & Dewitte, B. ENSO regimes: Reinterpreting the canonical and Modoki El Niño. *Geophysical Research Letters* **38**, doi:10.1029/2011gl047364 (2011).

9 Tziperman, E. & Yu, L. S. Quantifying the dependence of westerly wind bursts on the large-scale tropical Pacific SST. *Journal of Climate* **20**, 2760-2768, doi:10.1175/jcli4138.1 (2007).

10 Lengaigne, M. *et al.* Triggering of El Niño by westerly wind events in a coupled general circulation model. *Climate Dynamics* **23**, 601-620, doi:10.1007/s00382-004-0457-2 (2004).

11 Choi, J., An, S. I. & Yeh, S. W. Decadal amplitude modulation of two types of ENSO and its relationship with the mean state. *Climate Dynamics* **38**, 2631-2644, doi:10.1007/s00382-011-1186-y (2012).

12 L'Heureux, M. L. *et al.* Observing and predicting the 2015/16 El Niño. *Bulletin of the American Meteorological Society* **98**, 1363-1382, doi:10.1175/bams-d-16-0009.1 (2017).

13 Jin, F. F., Kim, S. T. & Bejarano, L. A coupled-stability index for ENSO. *Geophysical Research Letters* **33**, doi:10.1029/2006gl027221 (2006).

14 Hoerling, M. P. & Kumar, A. Why do North American climate anomalies differ from one El Niño event to another? *Geophysical Research Letters* **24**, 1059-1062, doi:10.1029/97gl00918 (1997).

15 Karoly, D. J. & Hoskins, B. J. 3 dimensional Propagation of Planetary Waves. *Journal of the Meteorological Society of Japan* **60**, 109-123 (1982).

16 Ropelewski, C. F. & Halpert, M. S. Global and Regional Scale Precipitation Patterns associated with the El-Niño Southern Oscillation. *Monthly Weather Review* **115**, 1606-1626, (1987).

17 Larkin, N. K. & Harrison, D. E. On the definition of El Niño and associated seasonal average US weather anomalies. *Geophysical Research Letters* **32**, 4, doi:10.1029/2005gl022738 (2005).

18 Cobb, K. M. *et al.* Highly Variable El Niño-Southern Oscillation Throughout the Holocene. *Science* **339**, 67-70, doi:10.1126/science.1228246 (2013).

19 McGregor, S., Timmermann, A., England, M. H., Timm, O. E. & Wittenberg, A. T. Inferred changes in El Niño-Southern Oscillation variance over the past six centuries. *Climate of the Past* **9**, 2269-2284, doi:10.5194/cp-9-2269-2013 (2013).

Documents using multi-proxy data that ENSO variance has increased over the past Century, relative to the 500 years prior to this.

20 Cai, W. J. *et al.* ENSO and greenhouse warming. *Nature Climate Change* **5**, 849-859, doi:10.1038/nclimate2743 (2015).

21 Rasmusson, E. M. & Carpenter, T. H. Variations in Tropical Sea-Surface Temperature and Surface Wind Fields associated with the Southern Oscillation El-Niño. *Monthly Weather Review* **110**, 354-384, (1982).

22 Wang, C. Z. On the ENSO mechanisms. *Advances in Atmospheric Sciences* **18**, 674-691 (2001).

23 Jin, F. F. An equatorial ocean recharge paradigm for ENSO. Part I: Conceptual model. *Journal of the Atmospheric Sciences* **54**, 811-829, (1997).

Introduces heuristic model that explains key features of ENSO dynamics, such as the important role of recharge and discharge processes in ENSO.

24 Roberts, A., Guckenheimer, J., Widiasih, E., Timmermann, A. & Jones, C. Mixed-Mode Oscillations of El Niño-Southern Oscillation. *Journal of the Atmospheric Sciences* **73**, 1755-1766, doi:10.1175/jas-d-15-0191.1 (2016).

25 Levine, A. F. Z. & Jin, F. F. Noise-Induced Instability in the ENSO Recharge Oscillator. *Journal of the Atmospheric Sciences* **67**, 529-542, doi:10.1175/2009jas3213.1 (2010).

26 Rayner, N. A. *et al.* Global analyses of sea surface temperature, sea ice, and night marine air temperature since the late nineteenth century. *Journal of Geophysical Research-Atmospheres* **108**, 4407, doi:10.1029/2002jd002670 (2003).

27 Giese, B. S. & Ray, S. El Niño variability in simple ocean data assimilation (SODA), 1871-2008. *Journal of Geophysical Research-Oceans* **116**, doi:10.1029/2010jc006695 (2011).

28 Johnson, N. C. How Many ENSO Flavors Can We Distinguish? *Journal of Climate* **26**, 4816-4827, doi:10.1175/jcli-d-12-00649.1 (2013).

29 Kug, J. S. & Ham, Y. G. Are there two types of La Niña? *Geophysical Research Letters* **38**, doi:10.1029/2011gl048237 (2011).

30 Kao, H. Y. & Yu, J. Y. Contrasting Eastern-Pacific and Central-Pacific Types of ENSO. *Journal of Climate* **22**, 615-632, doi:10.1175/2008jcli2309.1 (2009).

31 Lengaigne, M. & Vecchi, G. A. Contrasting the termination of moderate and extreme El Nio events in coupled general circulation models. *Climate Dynamics* **35**, 299-313, doi:10.1007/s00382-009-0562-3 (2010).

32 An, S.-I., Kug, J.-S., Timmermann, A., Kang, I.-S. & Timm, O. The influence of ENSO on the generation of decadal variability in the North Pacific. *Journal of Climate* **20**, 667-680, doi:10.1175/JCLI4017.1 (2007).

33 Deser, C., Simpson, I. R., McKinnon, K. A. & Phillips, A. S. The Northern Hemisphere Extratropical Atmospheric Circulation Response to ENSO: How Well Do We Know It and How Do We Evaluate Models Accordingly? *Journal of Climate* **30**, 5059-5082, doi:10.1175/jcli-d-16-0844.1 (2017).

34 Fedorov, A. V., Hu, S. N., Lengaigne, M. & Guilyardi, E. The impact of westerly wind bursts and ocean initial state on the development, and diversity of El Niño events. *Climate Dynamics* **44**, 1381-1401, doi:10.1007/s00382-014-2126-4 (2015).

35 Seiki, A. & Takayabu, Y. N. Westerly wind bursts and their relationship with intraseasonal variations and ENSO. Part I: Statistics. *Monthly Weather Review* **135**, 3325-3345, doi:10.1175/mwr3477.1 (2007).

36 Jin, F. F., Lin, L., Timmermann, A. & Zhao, J. Ensemble-mean dynamics of the ENSO recharge oscillator under state-dependent stochastic forcing. *Geophysical Research Letters* **34**, L03807, doi:10.1029/2006gl027372 (2007).

37 Vimont, D. J., Battisti, D. S. & Hirst, A. C. The seasonal footprinting mechanism in the CSIRO general circulation models. *Journal of Climate* **16**, 2653-2667, (2003).

Presents a coupled air-sea mechanisms by which extratropical Pacific climate anomalies can propagate into the tropics

38 Hong, L. C., LinHo & Jin, F. F. A Southern Hemisphere booster of super El Niño. *Geophysical Research Letters* **41**, 2142-2149, doi:10.1002/2014gl059370 (2014).

39 Ham, Y. G., Kug, J. S., Park, J. Y. & Jin, F. F. Sea surface temperature in the north tropical Atlantic as a trigger for El Niño/Southern Oscillation events. *Nature Geoscience* **6**, 112-116, doi:10.1038/ngeo1686 (2013).

40 Chikamoto, Y. *et al.* Skilful multi-year predictions of tropical trans-basin climate variability. *Nature Communications* **6**, doi:10.1038/ncomms7869 (2015).

Documents the impact of Atlantic SST anomalies on the generation of CP El Niño events

41 Yu, J. Y. & Kim, S. T. Relationships between Extratropical Sea Level Pressure Variations and the Central Pacific and Eastern Pacific Types of ENSO. *Journal of Climate* **24**, 708-720, doi:10.1175/2010jcli3688.1 (2011).

42 Lee, T. & McPhaden, M. J. Increasing intensity of El Niño in the central-equatorial Pacific. *Geophysical Research Letters* **37**, doi:10.1029/2010gl044007 (2010).

43 Wittenberg, A. T., Rosati, A., Delworth, T. L., Vecchi, G. A. & Zeng, F. R. ENSO Modulation: Is It Decadally Predictable? *Journal of Climate* **27**, 2667-2681, doi:10.1175/jcli-d-13-00577.1 (2014).

44 Yeh, S. W. *et al.* El Niño in a changing climate. *Nature* **461**, 511-U570, doi:10.1038/nature08316 (2009).

45 Capotondi, A. & Sardeshmukh, P. D. Optimal precursors of different types of ENSO events. *Geophysical Research Letters* **42**, 9952-9960, doi:10.1002/2015gl066171 (2015).

46 Xie, R. & Jin, F.-F. Two Leading ENSO Modes and El Niño Types in the Zebiak- Cane Model *Journal of Climate*, doi:10.1175/JCLI- D- 1117- 0469.1 (2018)

Theoretical evidence for two coupled modes which resemble EP and CP El Niño events with different timescales and background state sensitivities

47 Ham, Y. G. & Kug, J. S. How well do current climate models simulate two types of El Niño? *Climate Dynamics* **39**, 383-398, doi:10.1007/s00382-011-1157-3 (2012).

Shows that the current generation of climate models tends to underestimate diversity of El Niño due dry and cold biases in the equatorial central Pacific

48 Bellenger, H., Guilyardi, E., Leloup, J., Lengaigne, M. & Vialard, J. ENSO representation in climate models: from CMIP3 to CMIP5. *Climate Dynamics* **42**, 1999-2018, doi:10.1007/s00382-013-1783-z (2014).

49 Bayr, T. *et al.* Mean-state dependence of ENSO atmospheric feedbacks in climate models. *Climate Dynamics*, 10.1007/s00382-00017-03799-00382 (2017).

50 Li, T. Phase transition of the El Niño Southern oscillation: A stationary SST mode. *Journal of the Atmospheric Sciences* **54**, 2872-2887 (1997).

Applies seasonally varying instability to model of coupled ENSO dynamics.

51 Zhang, W. J. *et al.* Unraveling El Niño's impact on the East Asian Monsoon and Yangtze River summer flooding. *Geophysical Research Letters* **43**, 11375-11382, doi:10.1002/2016gl071190 (2016).

52 Trenberth, K. E. *et al.* Progress during TOGA in understanding and modeling global teleconnections associated with tropical sea surface temperatures. *Journal of Geophysical Research-Oceans* **103**, 14291-14324, doi:10.1029/97jc01444 (1998).

53 Risbey, J. S., Pook, M. J., McIntosh, P. C., Wheeler, M. C. & Hendon, H. H. On the Remote Drivers of Rainfall Variability in Australia. *Monthly Weather Review* **137**, 3233-3253, doi:10.1175/2009mwr2861.1 (2009).

54 McPhaden, M. J. Genesis and evolution of the 1997-98 El Niño. *Science* **283**, 950-954, doi:10.1126/science.283.5404.950 (1999).

55 Vecchi, G. A. & Harrison, D. E. Tropical Pacific sea surface temperature anomalies, El Niño, and equatorial westerly wind events. *Journal of Climate* **13**, 1814-1830, (2000).

56 Wengel, C., Latif, M., Park, W., Harlass, J. & Bayr, T. Seasonal ENSO phase locking in the Kiel Climate Model: The importance of the equatorial cold sea surface temperature bias. *Climate Dynamics*, doi:10.1007/s00382-00017-03648-00383 (2017).

57 Zebiak, S. E. & Cane, M. A. A Model El-Niño Southern Oscillation. *Monthly Weather Review* **115**, 2262-2278, (1987).

58 Tziperman, E., Zebiak, S. E. & Cane, M. A. Mechanisms of seasonal - ENSO interaction. *Journal of the Atmospheric Sciences* **54**, 61-71, (1997).

59 Galanti, E. *et al.* The equatorial thermocline outcropping - A seasonal control on the tropical Pacific Ocean-atmosphere instability strength. *Journal of Climate* **15**, 2721-2739, (2002).

60 Dommenget, D. & Yu, Y. S. The seasonally changing cloud feedbacks contribution to the ENSO seasonal phase-locking. *Climate Dynamics* **47**, 3661-3672, doi:10.1007/s00382-016-3034-6 (2016).

61 Harrison, D. E. & Vecchi, G. A. On the termination of El Niño. *Geophysical Research Letters* **26**, 1593-1596, doi:10.1029/1999gl900316 (1999).

62 Lengaigne, M., Boulanger, J. P., Menkes, C. & Spencer, H. Influence of the seasonal cycle on the termination of El Niño events in a coupled general circulation model. *Journal of Climate* **19**, 1850-1868, doi:10.1175/jcli3706.1 (2006).

63 McGregor, S., Timmermann, A., Schneider, N., Stuecker, M. F. & England, M. H. The Effect of the South Pacific Convergence Zone on the Termination of El Niño Events and the Meridional Asymmetry of ENSO. *Journal of Climate* **25**, 5566-5586, doi:10.1175/jcli-d-11-00332.1 (2012).

Demonstrates that the southward wind-shift that leads to rapid decay of El Niño events is related to the seasonal formation of the South Pacific Convergence Zone

64 Stuecker, M. F., Timmermann, A., Jin, F. F., McGregor, S. & Ren, H. L. A combination mode of the annual cycle and the El Niño/Southern Oscillation. *Nature Geoscience* **6**, 540-544, doi:10.1038/ngeo1826 (2013).

65 Stuecker, M. F., Jin, F. F., Timmermann, A. & McGregor, S. Combination Mode Dynamics of the Anomalous Northwest Pacific Anticyclone. *Journal of Climate* **28**, 1093-1111, doi:10.1175/jcli-d-14-00225.1 (2015).

66 Meinen, C. S. & McPhaden, M. J. Observations of warm water volume changes in the equatorial Pacific and their relationship to El Niño and La Niña. *Journal of Climate* **13**, 3551-3559, (2000).

67 Barnston, A., Tippett, M. K., Ranganathan, M. & L'Heureux, M. Deterministic skill of ENSO predictions from the North American Multimodel Ensemble *Climate Dynamics,* doi: 10.1007/s00382-017-3603-3, (2017).

68 Ramesh, N. & Murtugudde, R. All flavours of El Niño have similar early subsurface origins. *Nature Climate Change* **3**, 42-46 (2013).

69 Ballester, J., Bordoni, S., Petrova, D. & Rodo, X. Heat advection processes leading to El Niño events as depicted by an ensemble of ocean assimilation products. *Journal of Geophysical Research-Oceans* **121**, 3710-3729, doi:10.1002/2016jc011718 (2016).

70 Izumo, T. *et al.* Influence of the state of the Indian Ocean Dipole on the following year's El Niño. *Nature Geoscience* **3**, 168-172, doi:10.1038/ngeo760 (2010).

71 Ham, Y. G., Kug, J. S. & Park, J. Y. Two distinct roles of Atlantic SSTs in ENSO variability: North Tropical Atlantic SST and Atlantic Niño. *Geophysical Research Letters* **40**, 4012-4017, doi:10.1002/grl.50729 (2013).

72 Takahashi, K. & Dewitte, B. Strong and moderate nonlinear El Niño regimes. *Climate Dynamics* **46**, 1627-1645, doi:10.1007/s00382-015-2665-3 (2016).

73 Barnston, A. G., Tippett, M. K., L'Heureux, M. L., Li, S. H. & DeWitt, D. G. Skill of Real-Time Seasonal ENSO Model Predictions during 2002-11: Is Our Capability Increasing? *Bulletin of the American Meteorological Society* **93**, 631-651, doi:10.1175/bams-d-11-00111.1 (2012).

74 Newman, M. & Sardeshmukh, P. D. Are we near the predictability limit of tropical Indo-Pacific sea surface temperatures? *Geophysical Research Letters* **44**, 8520-8529, doi:10.1002/2017gl074088 (2017).

75 Petrova, D., Koopman, S. J., Ballester, J. & Rodo, X. Improving the long-lead predictability of El Nio using a novel forecasting scheme based on a dynamic components model. *Climate Dynamics* **48**, 1249-1276, doi:10.1007/s00382-016-3139-y (2017).

76 Kessler, W. S. Is ENSO a cycle or a series of events? *Geophysical Research Letters* **29**, doi:10.1029/2002gl015924 (2002).

Challenges the notion of ENSO as a cycle and highlights the fact that the ENSO system can loose its dynamical memory during long La Niña events

77 Barnston, A. G. & Tippett, M. K. Do Statistical Pattern Corrections Improve Seasonal Climate Predictions in the North American Multimodel Ensemble Models? *Journal of Climate* **30**, 8335-8355, doi:10.1175/jcli-d-17-0054.1 (2017).

78 DiNezio, P. N., Deser, C., Okumura, Y. & Karspeck, A. Predictability of 2-year La Nia events in a coupled general circulation model. *Climate Dynamics* **49**, 4237-4261, doi:10.1007/s00382-017-3575-3 (2017).

79 McPhaden, M. J. A 21st century shift in the relationship between ENSO SST and warm water volume anomalies. *Geophysical Research Letters* **39**, doi:10.1029/2012gl051826 (2012).

80 Jeong, H. I. *et al.* Assessment of the APCC coupled MME suite in predicting the distinctive climate impacts of two flavors of ENSO during boreal winter. *Climate Dynamics* **39**, 475-493, doi:10.1007/s00382-012-1359-3 (2012).

81 Larson, S. & Kirtman, B. The Pacific Meridional Mode as a trigger for ENSO in a high-resolution coupled model. *Geophysical Research Letters* **40**, 3189-3194, doi:10.1002/grl.50571 (2013).

82 Zhang, H. H., Clement, A. & Di Nezio, P. The South Pacific Meridional Mode: A Mechanism for ENSO-like Variability. *Journal of Climate* **27**, 769-783, doi:10.1175/jcli-d-13-00082.1 (2014).

83 An, S. I. Interannual variations of the Tropical Ocean instability wave and ENSO. *Journal of Climate* **21**, 3680-3686, doi:10.1175/2008jcli1701.1 (2008).

84 Larson, S. M. & Kirtman, B. P. Linking preconditioning to extreme ENSO events and reduced ensemble spread. *Climate Dynamics*, doi:10.1007/s00382-00017-03791-x (2017).

85 Chen, N. & Majda, A. J. Simple dynamical models capturing the key features of the Central Pacific El Niño. *Proceedings of the National Academy of Sciences of the United States of America* **113**, 11732-11737, doi:10.1073/pnas.1614533113 (2016).

86 Hao, Z., Neelin, J. D. & Jin, F. F. Nonlinear Tropical Air-Sea Interaction in the Fast-Wave Limit. *Journal of Climate* **6**, 1523-1544, (1993).

87 Schneider, N. The response of tropical climate to the equatorial emergence of spiciness anomalies. *Journal of Climate* **17**, 1083-1095, (2004).

88 McGregor, S., Sen Gupta, A., Holbrook, N. J. & Power, S. B. The Modulation of ENSO Variability in CCSM3 by Extratropical Rossby Waves. *Journal of Climate* **22**, 5839-5853, doi:10.1175/2009jcli2922.1 (2009).

89 Xue, Y. *et al.* A real-time ocean reanalyses intercomparison project in the context of tropical pacific observing system and ENSO monitoring. *Climate Dynamics* **49**, 3647-3672, doi:10.1007/s00382-017-3535-y (2017).

90 Widlansky, M. J. *et al.* Changes in South Pacific rainfall bands in a warming climate. *Nature Climate Change* **3**, 417-423, doi:10.1038/NCLIMATE1726 (2013).

91 Kirtman, B. P., Straus, D. M., Min, D. H., Schneider, E. K. & Siqueira, L. Toward linking weather and climate in the interactive ensemble NCAR climate model. *Geophysical Research Letters* **36**, doi:10.1029/2009gl038389 (2009).

92 Vecchi, G. A. *et al.* On the Seasonal Forecasting of Regional Tropical Cyclone Activity. *Journal of Climate* **27**, 7994-8016, doi:10.1175/jcli-d-14-00158.1 (2014).

93 Cook, E. R., Seager, R., Cane, M. A. & Stahle, D. W. North American drought: Reconstructions, causes, and consequences. *Earth-Science Reviews* **81**, 93-134, doi:10.1016/j.earscirev.2006.12.002 (2007).

94 Nicholson, S. E. & Selato, J. C. The influence of La Niña on African rainfall. *International Journal of Climatology* **20**, 1761-1776, (2000).

95 McPhaden, M. J., Zebiak, S. E. & Glantz, M. H. ENSO as an integrating concept in Earth science. *Science* **314**, 1740-1745, doi:10.1126/science.1132588 (2006).

96 Balmaseda, M. A., Mogensen, K. & Weaver, A. T. Evaluation of the ECMWF ocean reanalysis system ORAS4. *Quarterly Journal of the Royal Meteorological Society* **139**, 1132-1161, doi:10.1002/qj.2063 (2013).

97 Huang, B. Y. *et al.* Extended Reconstructed Sea Surface Temperature, Version 5 (ERSSTv5): Upgrades, Validations, and Intercomparisons. *Journal of Climate* **30**, 8179-8205, doi:10.1175/jcli-d-16-0836.1 (2017).

98 Penny, S. G., Behringer, D. W., Carton, J. A. & Kalnay, E. A Hybrid Global Ocean Data Assimilation System at NCEP. *Monthly Weather Review* **143**, 4660-4677, doi:10.1175/mwr-d-14-00376.1 (2015).

99 Puy, M., Vialard, J., Lengaigne, M. & Guilyardi, E. Modulation of equatorial Pacific westerly/easterly wind events by the Madden-Julian oscillation and convectively-coupled Rossby waves. *Climate Dynamics* **46**, 2155-2178, doi:10.1007/s00382-015-2695-x (2016).

100 Adler, R. F. *et al.* The version-2 global precipitation climatology project (GPCP) monthly precipitation analysis (1979-present). *Journal of Hydrometeorology* **4**, 1147-1167, (2003).

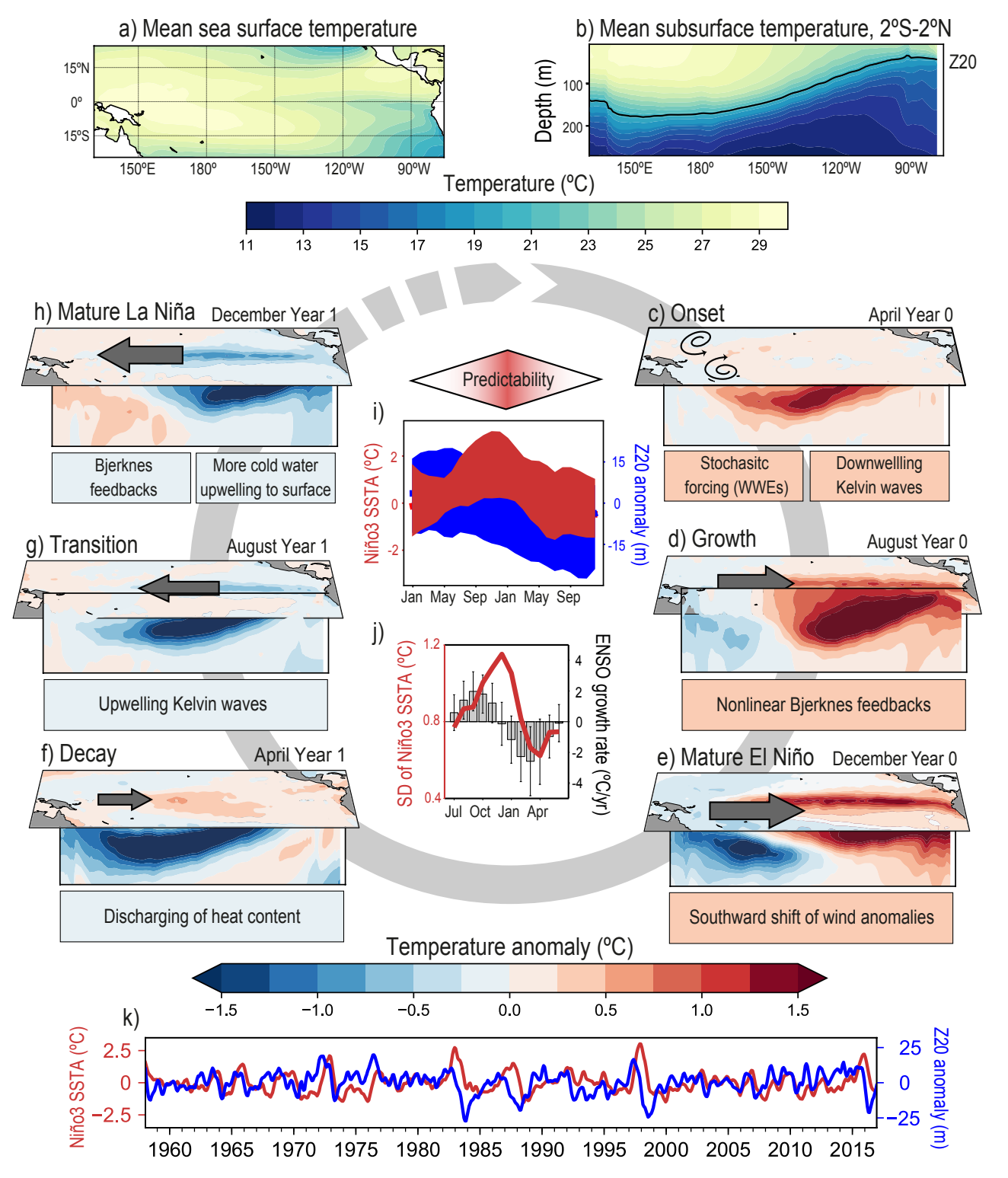
a) Mean sea surface temperature
15°N
0°
15°S
150°E
180°
150°W
120°W
90°W
b) Mean subsurface temperature, 2°S-2°N
Depth (m)
100
200
Z20
150°E
180°
150°W
120°W
90°W
Temperature (°C)
11
13
15
17
19
21
23
25
27
29
h) Mature La Niña
December Year 1
Bjerknes feedbacks
More cold water upwelling to surface
c) Onset
April Year 0
Stochasitc forcing (WWEs)
Downwellling Kelvin waves
Predictability
i)
Niño3 SSTA (°C)
2
0
-2
Z20 anomaly (m)
15
0
-15
Jan May Sep Jan May Sep
g) Transition
August Year 1
Upwelling Kelvin waves
d) Growth
August Year 0
Nonlinear Bjerknes feedbacks
j)
SD of Niño3 SSTA (°C)
1.2
0.8
0.4
ENSO growth rate (°C/yr)
4
2
0
-2
-4
Jul Oct Jan Apr
f) Decay
April Year 1
Discharging of heat content
e) Mature El Niño
December Year 0
Southward shift of wind anomalies
Temperature anomaly (°C)
−1.5
−1.0
−0.5
0.0
0.5
1.0
1.5
k)
Niño3 SSTA (°C)
2.5
0
−2.5
Z20 anomaly (m)
25
0
−25
1960
1965
1970
1975
1980
1985
1990
1995
2000
2005
2010
2015

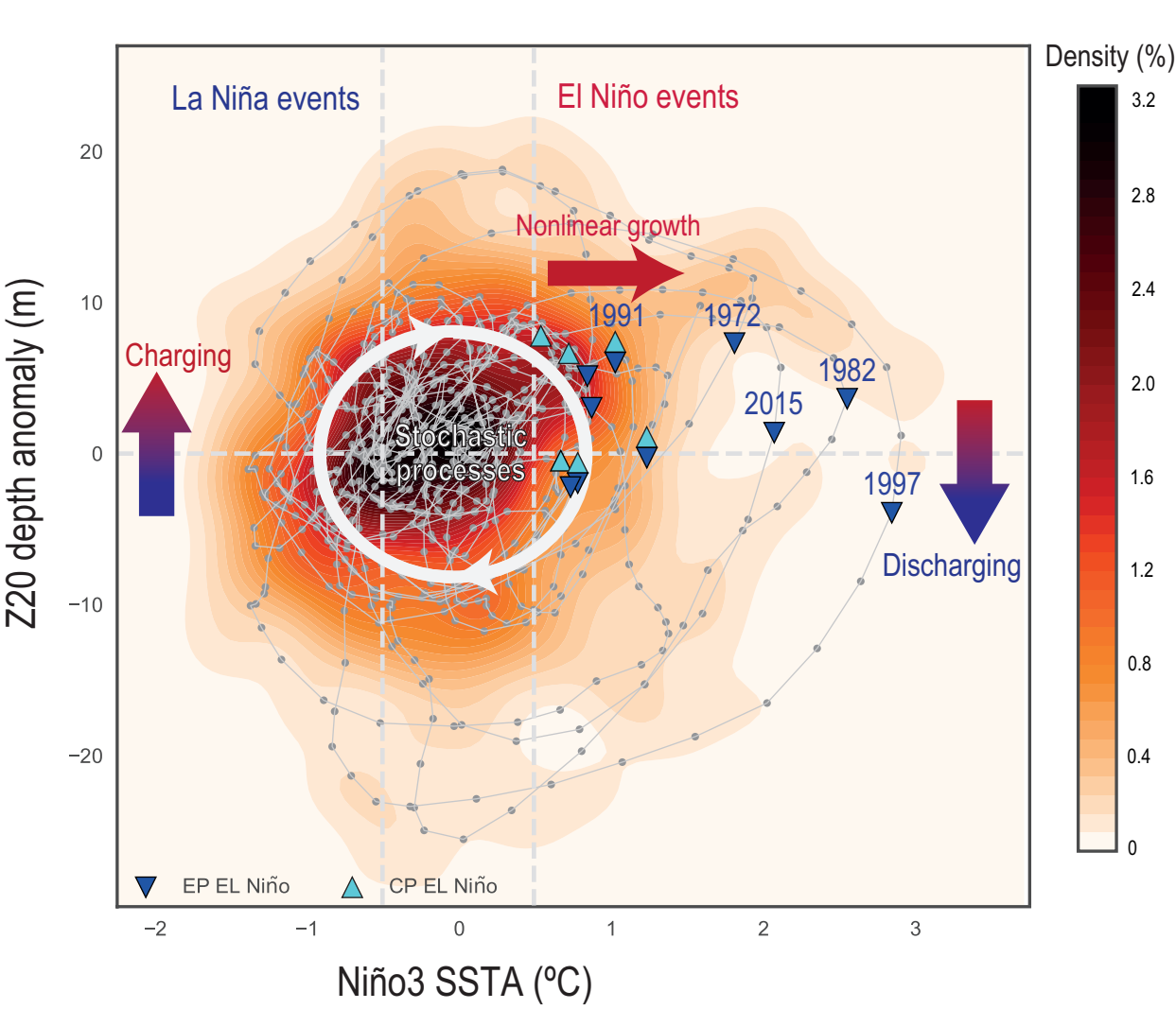
La Niña events
El Niño events
Nonlinear growth
Charging
Discharging
Stochastic processes
1991
1972
1982
2015
1997
EP EL Niño
CP EL Niño
Z20 depth anomaly (m)
Niño3 SSTA (ºC)
Density (%)
3.2
2.8
2.4
2.0
1.6
1.2
0.8
0.4
0
20
10
0
−10
−20
−2
−1
0
1
2
3

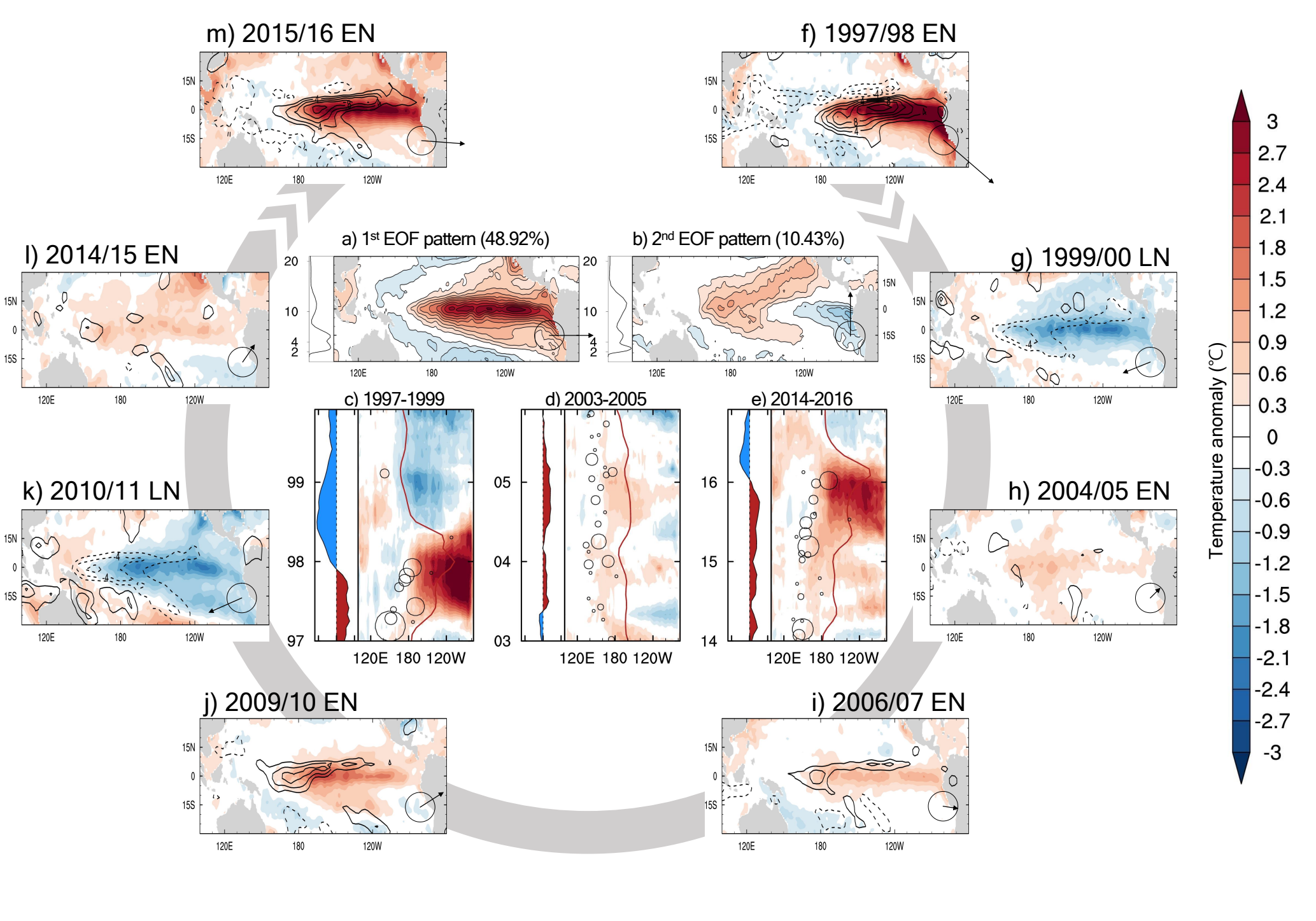
m) 2015/16 EN
f) 1997/98 EN
l) 2014/15 EN
a) 1st EOF pattern (48.92%)
b) 2nd EOF pattern (10.43%)
g) 1999/00 LN
c) 1997-1999
d) 2003-2005
e) 2014-2016
k) 2010/11 LN
h) 2004/05 EN
j) 2009/10 EN
i) 2006/07 EN
120E
180
120W
15N
0
15S
Temperature anomaly (°C)
3
2.7
2.4
2.1
1.8
1.5
1.2
0.9
0.6
0.3
0
-0.3
-0.6
-0.9
-1.2
-1.5
-1.8
-2.1
-2.4
-2.7
-3

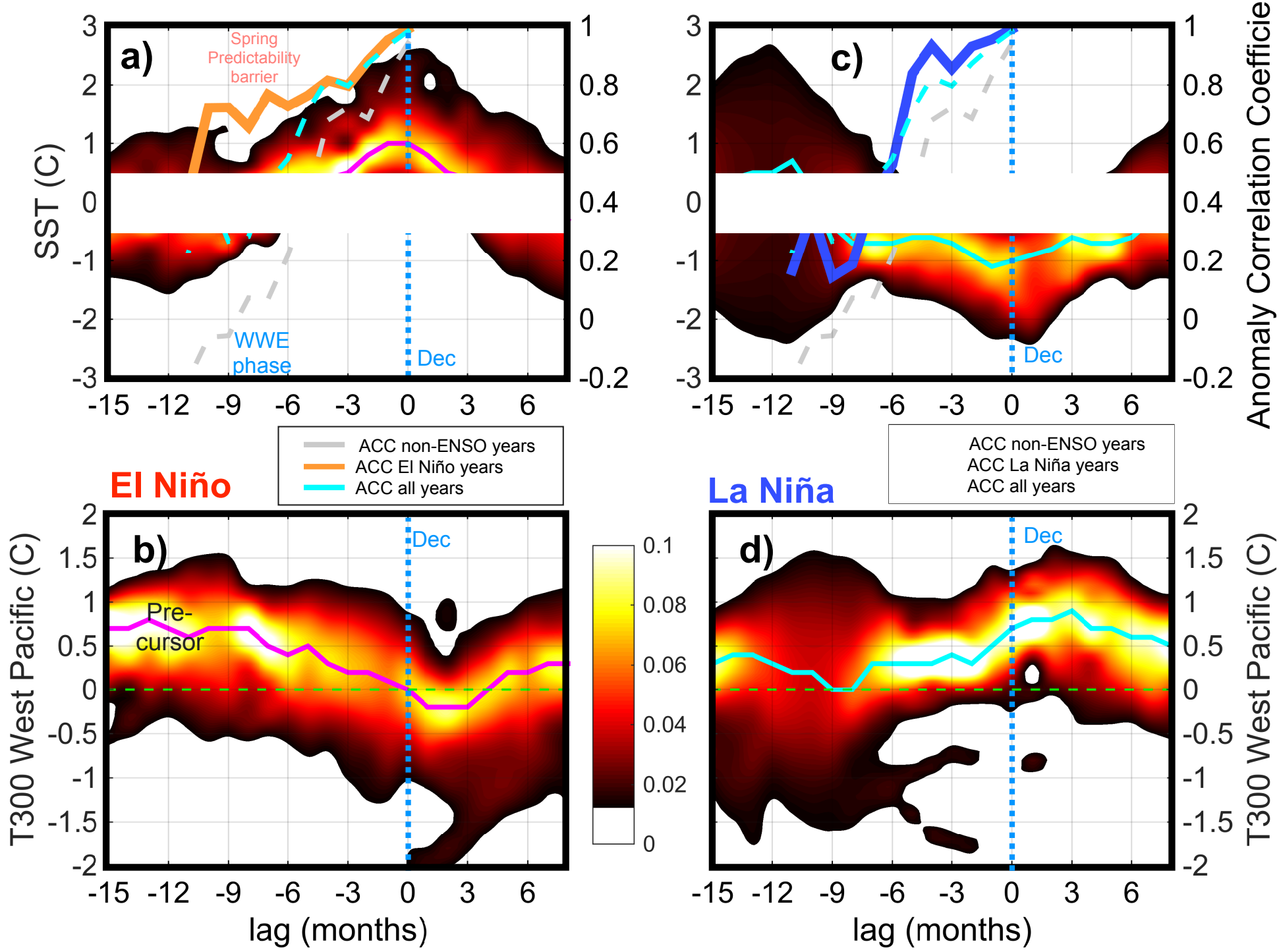
a)
Spring
Predictability
barrier
WWE
phase
Dec
SST (C)
c)
Dec
Anomaly Correlation Coefficient
ACC non-ENSO years
ACC El Niño years
ACC all years
El Niño
ACC non-ENSO years
ACC La Niña years
ACC all years
La Niña
b)
Pre-
cursor
Dec
T300 West Pacific (C)
lag (months)
d)
Dec
T300 West Pacific (C)
lag (months)

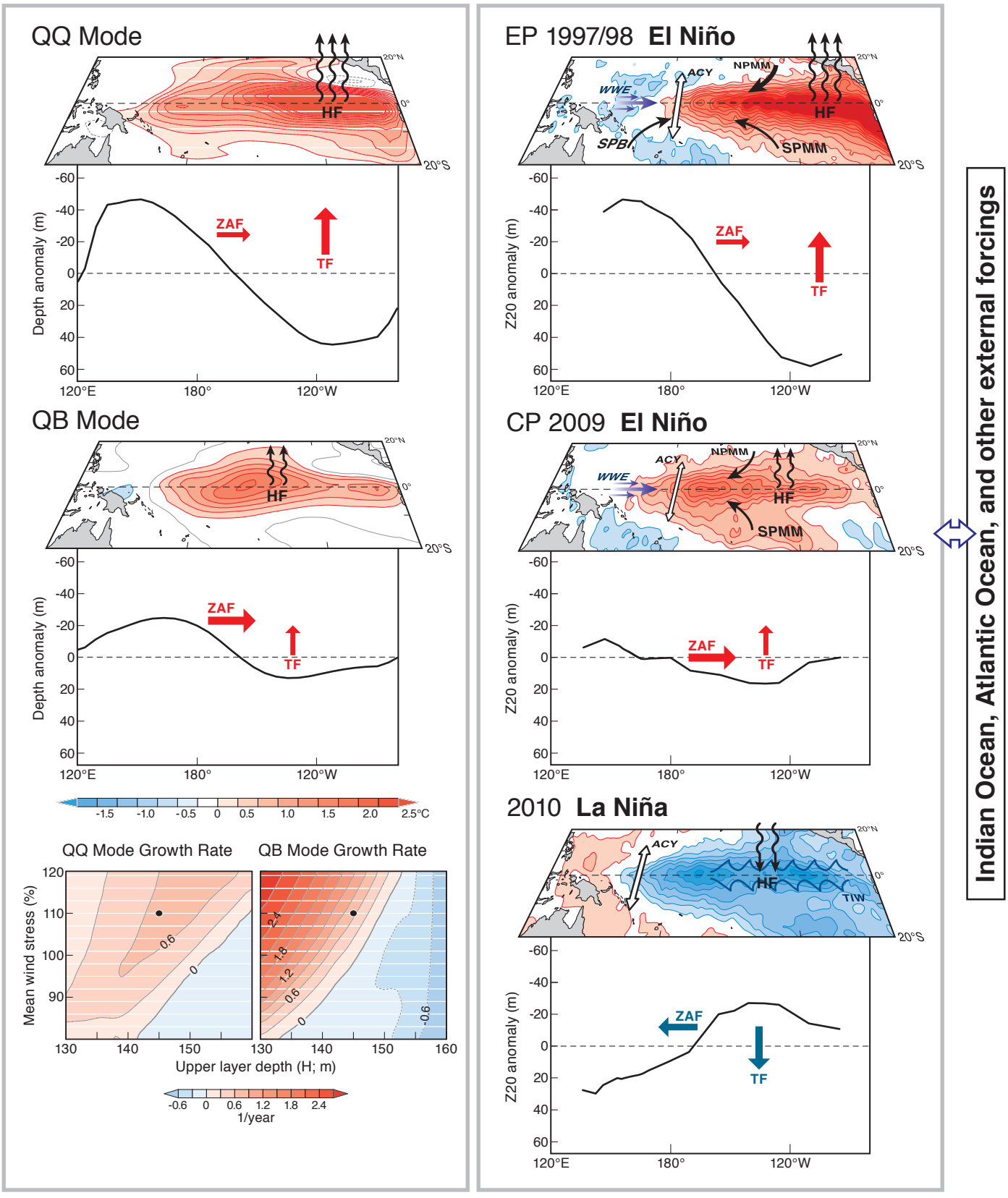
QQ Mode
HF
20°N
0°
20°S
Depth anomaly (m)
ZAF
TF
120°E
180°
120°W
QB Mode
EP 1997/98 El Niño
ACY
NPMM
WWE
SPBI
SPMM
Z20 anomaly (m)
CP 2009 El Niño
2010 La Niña
TIW
-1.5 -1.0 -0.5 0 0.5 1.0 1.5 2.0 2.5°C
QQ Mode Growth Rate
QB Mode Growth Rate
Mean wind stress (%)
Upper layer depth (H; m)
-0.6 0 0.6 1.2 1.8 2.4
1/year
Indian Ocean, Atlantic Ocean, and other external forcings